Journal of Materials and Environmental Science
ISSN : 2028-2508
e-ISSN : 2737-890X
CODEN : JMESCN

J. Mater. Environ. Sci., 2024, Volume 15, Issue 5, Page 674-687

http://www.jmaterenvironsci.com

Electrochemical aspects of copper atmospheric corrosion in a marine atmosphere abundant in hydrogen sulfide

Mahado SAID AHMED[1], Mounim LEBRINI[1, *]

[1] *Laboratoire des Matériaux et Molécules en Milieu Agressif, L3MA UR 4_1, Campus de Schœlcher, Université des Antilles*

**Corresponding author, Email address: mounim.lebrini@univ.antilles.fr;*

Received *29 Mar 2024,*
Revised *06 May 2024,*
Accepted *08 May 2024*

Citation*: Said Ahmed M., Lebrini M. (2024) Electrochemical aspects of copper atmospheric corrosion in a marine atmosphere abundant in hydrogen sulfide, J. Mater. Environ. Sci., 15(5), 674-687*

Abstract: This work investigates the influence of gases from biodegradation of *Sargassum algae*, in particular hydrogen sulphide (H_2S), on the atmospheric corrosion of copper. It has been shown that the presence of hydrogen sulphide from the biodegradation of stranded algae in the areas impacted by large arrivals plays an important role in the premature degradation/corrosion of common metals (e.g. connectors). This factor is added to other factors characteristic of a tropical marine atmosphere that is already very aggressive towards metallic materials (high TOW, sea spray loaded with Cl^- ions, constant and high temperatures throughout the year). This article presents a comparative electrochemical investigation into the atmospheric corrosion, rich in H_2S on copper at four sites in Martinique. This study discovered that the thickness loss values do not show a linear evolution, indicating a decrease in corrosion rate over time and suggesting the protective nature of the corrosion products on the surface. The observed sites exhibit significantly higher levels of corrosion compared to what is documented in existing literature. This serves as strong evidence of the highly corrosive nature of the atmospheres in Martinique towards materials. All electrochemical analyses (SIE and LP) conducted support the idea that the corrosion products formed on the surfaces are not protective. Instead, they enhance surface conductivity and accelerate the corrosion process. This effect is particularly pronounced at the Vauclin site, which may account for the elevated corrosion rates observed there.

Keywords: *Sargassum algae, H2S, Copper, Atmospheric corrosion, Electrochemical techniques*

1. Introduction

Copper is the preferred metallic material for fabricating multilevel interconnect structures in ultra-large scale integrated circuits owing to its superior electrical conductivity and high resistance to electromigration (Love *et al.,* 2005). Nonetheless, being an active metal, copper does not exhibit strong resistance to corrosion (Zschieschang *et al.,* 2010). Copper is considered a noble metal that can dissolve in harsh environments regardless of where it is used. While the formation of a protective oxide film

may give the impression that copper is corrosion-resistant in certain conditions or atmospheres, it actually oxidizes quickly in specific situations, leading to the creation of copper oxides and/or hydroxides on its surface. The type of film formed depends on the composition of the environment. Despite this natural protective film, copper can still corrode in acidic environments or in industrial settings that contain chloride, sulfate, or other ions (Dueke-Eze *et al.*, 2022), (Sedik *et al.,* 2022), (Pareek *et al.*, 2019), (Mihit *et al.*, 2006), (Dafali *et al.*, 2004) .

The corrosion of copper and copper alloys in atmospheric conditions has been extensively examined, encompassing investigations conducted in both real-world settings and controlled laboratory environments (Bai *et al.,* 2022), (Xuankai *et al.,* 2022), (Becke*r et al.,*2022), (Wan *et al.,*2019). It has been shown that the rate of atmospheric corrosion is primarily governed by the presence of pollutants in the atmosphere, as well as the influence of various factors such as temperature, relative humidity, precipitation, and wind (Leygraf *et al.,* 2016), (Cai *et al.,* 2018), (Feliu *et al.,* 1993), (Cramer *et al.,* 1990). Many authors have documented the composition of copper corrosion products formed in various atmospheric conditions (Kucera *et al.,* 1987), (Odnevall *et al.,* 1996), (Guttman, 1982), but only a limited number have studied corrosion product layers using electrochemical techniques.

This study is complementary to previous research on the corrosion of copper exposed to a marine atmosphere, whether rich or not in pollutants, particularly hydrogen sulfide (H_2S) originating from the decomposition of Sargassum algae.

The investigation employed methods such as mass loss measurement, Scanning Electron Microscopy/Energy Dispersive X-ray (SEM/EDX), and X-ray Diffraction (XRD) (Said Ahmed *et al*., 2023). This research exposed that the deposition of sargassum seaweed has a notable influence on the progression and structure of copper corrosion, primarily attributed to the release of hydrogen sulfide. In environments lacking substantial sargassum algae deposition, standard corrosion products (Cu_2O and $Cu_2Cl(OH)_3$) formed, and the corrosion rate closely resembled that observed in a typical tropical marine setting. Conversely, in areas heavily affected by *Sargassum algae* deposition (accompanied by the presence of H_2S), corrosion rates were markedly elevated. The resultant corrosion layer predominantly consisted of CuS, although the presence of hydroxylsulfate was also noted. The aim of the present paper is to present the electrochemical behavior and the anti-corrosive performance of the corrosion layer formed on the surface of the copper. EIS measurements and potentiodynamic polarization were carried out on the exposed surface after the different exposure periods.

2. **Methodology**

2.1 Selection of Sites, H_2S and Chlorides Ion Measurement Techniques

Selection of Sites: This study focused on four chosen locations*: Vert pré, Diamant, Vauclin, and Frégate est*. **Figure 1** illustrates their positions on the Martinique map. These sites, situated in a predominantly marine atmosphere with elevated chloride ion concentrations, vary in proximity to the seashore.

The temperature and relative humidity were consistently high (ranging from 25 °C to 35 °C and 75%) due to Martinique's geographical location. Consequently, the time of wetting (TOW), a crucial factor influencing copper corrosion, remained essentially uniform across the diverse sites. Considering the distance from the coast and the volume of Sargassum seaweed washed ashore, the sites can be ranked based on their susceptibility to H_2S generated from the decomposition of *Sargassum algae*, with Vert pré being the most affected, followed by Diamant, Vauclin, and Frégate est being the least impacted.

H_2S and Chloride ion measurements: Hydrogen Sulfide measurements were conducted using the Cairpol microsensor system, manufactured by Envea company in Poissy, France, as depicted in previous research (Said Ahmed et al., 2023). For chloride ion measurement, the sampling procedure adhered to the NF X 43-014 standard. Samples were collected using a cylindrical Owen-type plastic collector with ample height to prevent sample loss. Sampling occurred at regular intervals of every 30 days for subsequent analysis.

Figure 1. location of the different sites on the Martinique map

2.2 Sample preparation

The copper samples utilized in this study were of high purity, measuring 99.9% and having dimensions of 2 cm × 2.5 cm × 1 mm. Before exposure, all copper samples underwent a mechanical polishing process using 1200-grade SiC. Subsequently, they were rinsed with distilled water, dehydrated with ethanol and air-dried. Collection of samples occurred at intervals of 3, 6 and 12 months of exposure, providing a comprehensive understanding of the copper's response to the outdoor environment over time.

2.3 Electrochemical tests

The degradation of the material was assessed through two main electrochemical techniques. First, anodic and cathodic polarization curves were produced in a 3% sodium chloride solution at 25 °C under aerated conditions. These curves were obtained using a VMP3 potentiostat from Bio-Logic, employing a sweep rate of 10 mV/s. The experimental setup included a saturated calomel reference electrode, a platinum wire counter electrode, and copper specimen working electrodes. The second method involved electrochemical impedance spectroscopy measurements conducted in a Bio-Logic cell with three electrodes. The working electrodes comprised copper specimens with an exposed surface area of approximately 5 cm^2, submerged in a 3% sodium chloride electrolyte under aerated conditions. The counter electrode was made of high-purity (99.99%) platinum, and a saturated calomel electrode served

as the reference electrode. In both approaches, the open circuit potential (OCP) was continuously recorded until a steady state was achieved. Impedance plots were recorded in a frequency range from 200 kHz to 1 mHz, employing five points per decade and using a sinusoidal amplitude of 5 mV peak - to - peak at E = OCP. These tests were systematically repeated on three samples for each site and exposure period, ensuring the reliability and consistency of the obtained electrochemical data.

3. Results and Discussion

3.1 H_2S and Chloride ions Measurements and Determination of the Corrosion Rate

The concentrations of H_2S and chlorides in the atmosphere were continuously recorded at various sites throughout the copper exposure period. **Table 1** illustrates the monthly average variations in H_2S and chloride ion concentrations across different sites. The concentration of H_2S at the *Diamant* and *Vert pré* sites remained relatively low, around 10 ppb, attributed to the distance from *Sargassum algae* stranding areas. Conversely, at *Frégate est*, where sargassum stranding was observed, H_2S concentration was notably high, reaching approximately 2–4 ppm. Throughout the period, there was no significant seasonal fluctuation, suggesting the presence of algae throughout the year. In *Vauclin*, the impact of algae decomposition was less pronounced, with an annual average of 0.2 ppm. Regarding chloride concentration, the *Diamant* site (25 meters from the seashore) exhibited an exceptionally high value attributed to turbulent seas, causing the suspension of spray rich in sodium chloride. The lower concentrations observed in *Frégate est* and *Vert pré* can be attributed to wind direction and distance from the sea, respectively. Consequently, the corrosion process is likely influenced by H_2S emissions in *Frégate est* and by Chloride ion in *Diamant/Vert pré*. Regrettably, technical problems prevented the collection of chloride data from the Vauclin site. Nevertheless, it is reasonable to infer that the values would have been similar to those recorded in *Frégate est*.

Table 1. Average concentration of H_2S and chloride in different sites during 1-year exposure

Sites	**H_2S concentration**			**Cl^- concentration**		
	ppb			**mg l^{-1}**		
Months	3	6	12	3	6	12
Vert pré	20	16	12	13.6	18.7	7
Diamant	9	8	5	1780	144	92
Vauclin	250	220	200	-	-	-
Fregate est	4 150	2 820	2 590	71	27.8	10.3

Based on the above H_2S and chloride data, the atmospheres of Martinique can be classified into four distinct types.

- ✓ An atmosphere rich in H_2S but low in chloride (*Frégate est*)
- ✓ An atmosphere rich in chloride but low in H_2S (*Diamant*)
- ✓ An atmosphere poor in H_2S and chloride (*Vert pré*)
- ✓ An intermediate atmosphere, rich in H_2S (but less than that of Frégate est), and abundant in Cl^-, with a concentration comparable to Diamant (*Vauclin*).

3.2 Determination of the Corrosion Rate

The average thickness losses of copper exposed for 3 to 12 months at the four sites are summarized in **Table 2**. This is obtained by the difference between the initial mass and the mass after elimination of the corrosion products, taking into account the density of the copper. As show in the **Table 2**, the average thickness loss of copper samples at Frégate est is 15 times greater than that observed in *Diamant*. This clearly shows the major influence of gases produced by the decomposition of *Sargassum algae* on corrosion kinetics. However, when the samples are exposed far from the shores and areas heavily impacted by *Sargassum algae* strandings, as is the case with *Vert pré*, thickness losses are less significant and corrosion is less severe. The presence of both H_2S and Cl^- ions in the atmosphere in *Vauclin* leads to relatively high thickness losses. Since the influence of each of the corrosives cannot be clearly established, the hypothesis of a synergistic effect may be raised.

As described in the previous work (Said Ahmed *et al*., 2023), the thickness loss values do not show a linear evolution, indicating a decrease in corrosion rate over time and suggesting the protective nature of the corrosion products on the surface. The thickness loss follows a known logarithmic pattern and is consistent with previous research on copper (Cai *et al.,* 2020), (Vera *et al.,* 2017). This result suggests that corrosion dynamics depend solely on the material and not on environmental conditions. The values obtained are consistent with existing literature (Cai *et al.,* 2020) and confirm the protective characteristics of copper corrosion products.

Table 2. Average thickness loss of copper exposed in 4 sites for 3 to 12 months

Sites	**Thickness loss**		
	µm		
Months	3	6	12
Vert pré	2.3	3.7	4.8
Diamant	8	16.2	23
Vauclin	27.6	43.1	59.9
Fregate Est	120	256.3	328.8

3.3 Electrochemical measurements

To explore the electrochemical characteristics and corrosion resistance of the corrosion layer developed on copper surfaces, we conducted electrochemical impedance spectroscopy (EIS) measurements and potentiodynamic polarization on the exposed copper surfaces. The EIS data is presented through Nyquist and Bode plots, where the |Z| modulus and phase angle ϕ vary with the frequency domain. These plots are constructed in a complex plane format, relating to Zreal (Zr) and the imaginary part Zim (Zi). The interpretation of these plots involves employing a mathematical correlation to a specific physico-electrical model known as an equivalent electrical circuit (EEC). The EEC is constructed by arranging ideal components (resistors R and capacitors C) either in series or parallel to replicate the observed EIS spectra.

The Nyquist and Bode diagrams obtained for copper samples exposed to the atmosphere of Diamant for 3, 6, and 12 months are presented in **Figure 2a** and **Figure 3a**. These diagrams are obtained after 3 hours of open-circuit immersion. The electrolyte is a 3% NaCl solution maintained at 25°C. The electrochemical impedance diagrams of the non-exposed copper are characterized by two-time constants (Bode). Inspection of the EIS data obtained for the samples exposed for 3 months at

Diamant shows two capacitive loops (**Figure 2a**) with two-time constants in the Bode phase plots (**Figure 3a**). The first one is less pronounced than the second one. After 6 months of exposure, the two capacitive loops are well-pronounced. The significant increase in the sizes of the loops can be linked to the formation of a more compact corrosion layer on the substrate surface. This increase is supported by the decrease in the phase angle at 6 months (**Figure 3a**) which may also be associated with surface roughness. The increasing of the first capacitive loop can be explained by the growth of the $Cu_2O/CuCl(OH)_3$ corrosion layer (Said Ahmed *et al.*, 2023, Lu *et al*., 2021). Based on the studies carried out by Deslouis *& al*. and Gourbeyre *& al*. (Deslouis *et al*., 1988, Gourbeyre *et al.*, 2006), the behavior of the second capacitive loop would be related to a mass transport process together in the solution (associated to LF response of the EIS diagrams) and through the porous layer of the corrosion product. The impedance plots at Frégate est show two capacitive half-loops (**Figure 2b**) with two time constant very distinct in the Bode-phase plots (**Figure 3b**).

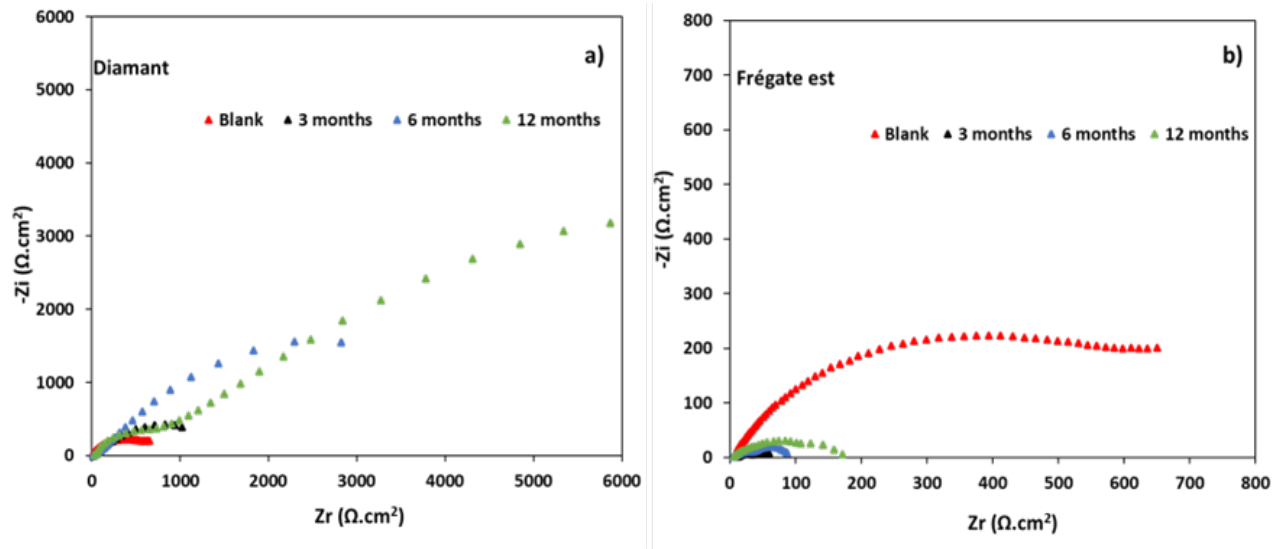

Figures 2. Nyquist plots in NaCl obtained for samples of Cu exposed in Diamant(a) and Frégate est (b)

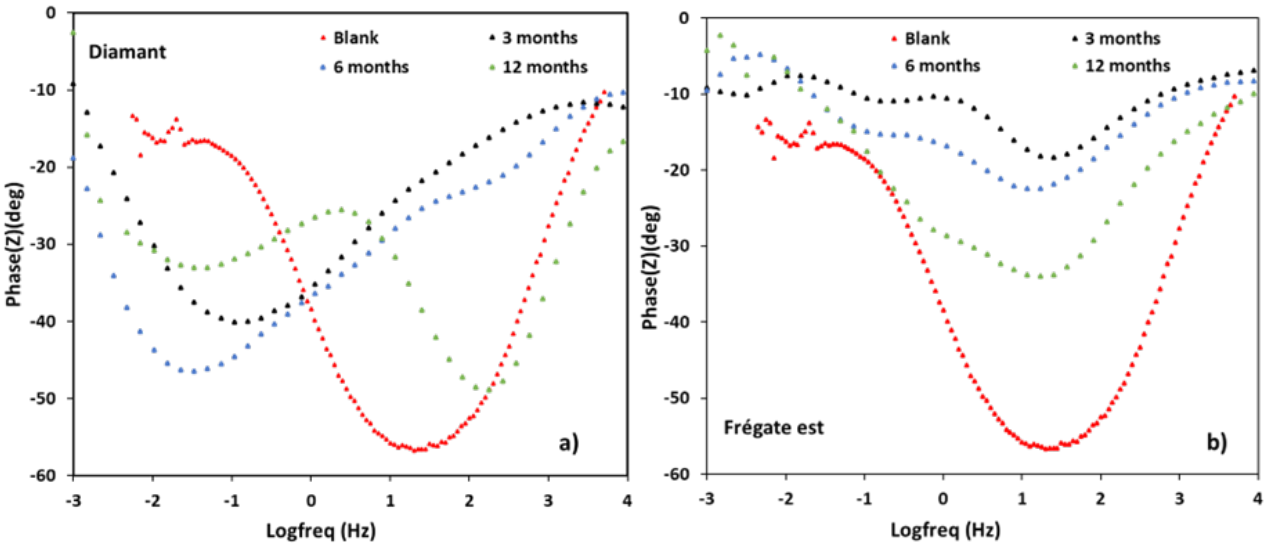

Figures 3. Bode plots in NaCl obtained for samples of Cu exposed in Vert Pré (a) and Vauclin (b)

We note that a similar electrochemical behavior was found for both exposure period. But the impedance decreases between the three periods indicating increased corrosion. The first impedance loop is associated with the behavior of the corrosion layer. Indeed, according to the previously work (Said Ahmed *et al.,* 2023), the loss of anticorrosion performance in corrosion products can be explained by the predominant presence of CuS. Indeed, similar to the samples exposed in *Diamant*, the first and second capacitive half-loops are associated, respectively, to the behavior of the corrosion layer and a charge transfer process. We note here that a blue coloration was observed during the electrochemical test. The blue colored in the cell can be attributed to the dissolution of copper sulfide in NaCl medium or/and indicated the formation of copper chloride in combination with copper oxide and hydroxide. Studies have found that in neutral chloride solutions the dominant corrosion product on the copper surface is CuCl, which eventually transforms into Cu_2O, which oxidizes to $Cu(OH)_2$, $Cu_2(OH)_3Cl \times Cu(OH)_2$. Several studies have found that in neutral chloride solutions the dominant corrosion product on the copper surface is CuCl, which eventually transforms into Cu_2O, which oxidizes to Cu $(OH)_2$, $Cu_2(OH)_3Cl \times Cu(OH)_2$ (Gourbeyre *et al.,* 2006).

The Nyquist plot acquired does not exhibit a perfectly formed semicircle. To compensate the depression of the semicircle caused by frequency dispersion in the experimental system—attributed to factors such as surface inhomogeneity, surface roughness, electrode porosity, surface disorder, geometric irregularities, and others-it is essential to substitute the capacitor (C) with a constant phase element (CPE). This adjustment aims to compensate for the observed deviations in the Nyquist plot. The CPE is defined in the impedance representation as:

$$Z_{CPE} = Q^{-1} (i\omega)^{-n} \qquad \textbf{Eqn. 1}$$

where Q = the CPE constant, ω = the angular frequency (in rad. s-1), i^2=-1 is the imaginary number and n = a CPE exponent.

Figure 4 illustrates the equivalent circuits employed for fitting the impedance data. A satisfactory fit with these models was achieved for our experimental data. As an illustration, the Nyquist and Bode diagrams comparing the experimental and fitted data with circuit are represented in **Figures 5a**. It is noticeable that a reasonably accurate fit was attained, as indicated by a Chi-square on the order of 10^{-3} for all experimental data.

The fitting parameters extracted from the Nyquist plots using EEC models are presented in **Table 3**. In this context, R_{total} is noted as the total resistance, defined as the sum of R_1 and R_2. It is evident that the values of R_{total} for the two sites (*Diamant/Fregate est*) are markedly different. In the absence of H_2S (*Diamant*), R_{total} progressively increases with the exposure time. This increase reflects the growing protective properties of the corrosion layer. Indeed, corrosion products, especially the p-type semiconductor Cu_2O compound, contribute to forming a layer with enhanced protective properties, thereby restricting access to the metal. Consequently, both the resistance of the corrosion layer and the charge transfer simultaneously increase. In an atmosphere rich in H_2S (*Fregate est*), the values of R_{total} are significantly lower.

This is attributed to the low resistances of the corrosion products, suggesting a lack of protection for the metal surface. These findings can be explained by the predominant presence of CuS (Said Ahmed *et al.,* 2023) a non-adherent and hygroscopic layer, that extends the wetting time of the surface and accelerates the corrosion process. Furthermore, **Table 4** indicates a regular variation in the values of Q with exposure time, demonstrating an observed decrease. These values remain very low for the second capacitive loop associated to a charge transfer.

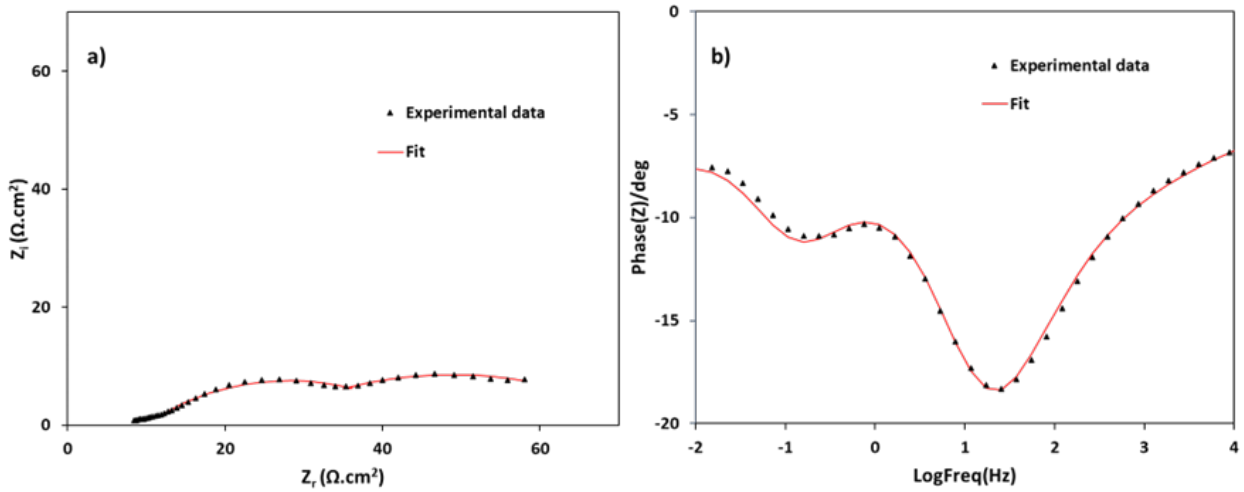

Figures 4. Complex plane impedance plot: (a) Nyquist plots; (b) Bode plots, (•) Experimental data and (▲) Fit data, together with the equivalent circuit used to fit the impedance data, recorded for copper at au *Frégate est* for 3 months

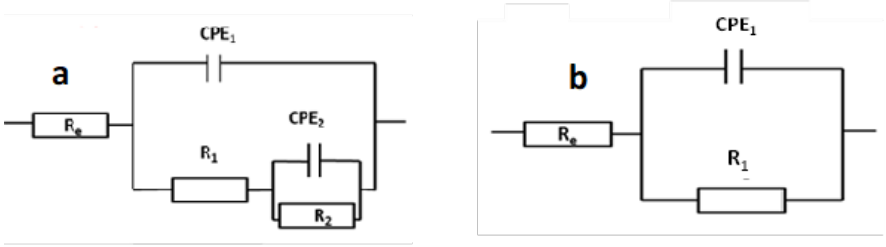

Figures 5. Equivalent electric circuit (EEC) used to fit experimental impedance data of exposed samples

The Table 4 also displays values of n below 1, which correspond to a constant phase element (CPE) behavior in the studied frequency range. A decrease in the values of n has been observed with exposure time, especially for the samples exposed to *Diamant*. n generally reflects the dispersion property of the corrosion current on the electrode surface: a low n value often indicates heterogeneous current distribution (Pawara *et al.,* 2007). This is particularly true when n values are below 0.95, as observed in this study, indicating the existence of damaged corrosion surfaces for both cases studied.

Table 3. Electrochemical parameters obtained for samples exposed in Vauclin and Vert.Pré at different exposure durations

	Blank	**Vert Pré**			**Vauclin**		
Months		3	6	12	3	6	12
R_e (Ω.cm²)	3	31	60	231	33	35	268
R_1(Ω.cm²)	–	2542	1243	746	544	970	6525
n_1	–	0.6831	0.6704	0.6384	0.7501	0.7237	0.7034
$Q_1 10^{-4}$ ($\Omega^{-1}cm^{-2}s^{n1}$)	–	3.6	7	6	7.3	6.4	0.93
R_2(Ω.cm²)	619	–	1757	3157	–	–	–
n_2	0.6978	–	0.7231	0.7354	–	–	–
$Q_2 10^{-4}$ ($\Omega^{-1}cm^{-2}s^{n2}$)	12	–	2.3	0.5	–	–	–

R_{total}(Ω.cm²)	619	2542	3000	3903	544	970	6527

The electrochemical behaviors of the samples exposed in two other atmospheres (*Vert Pré and Vauclin*) were studied under the same conditions. The Nyquist diagrams obtained for the samples exposed to *Vert pré* are represented in **Figure 6a**. After 3 months of exposure, a capacitive half-loop is observed, characterized by a time constant in the Bode plot (**Figure 7a**). this a single capacitive loop can be associated to the presence of a dense Cu_2O layer (Said Ahmed *et al.*, 2023). Additionally, the development of a second capacitive half-loop is observed, confirmed by the appearance of a second time constant (**Figure 7a**) at medium frequencies associated to charge transfer. An increase in the diameter of the capacitive half-loops over time is observed. It is noteworthy that this electrochemical behavior is similar to that of the samples exposed in *Diamant*. The decrease in the diameter of the capacitive half-loop after 6 months can be explained by the significant increase in the presence of the compound $Cu_2(OH)_3Cl$ in the layer (Said Ahmed *et al.*, 2023).

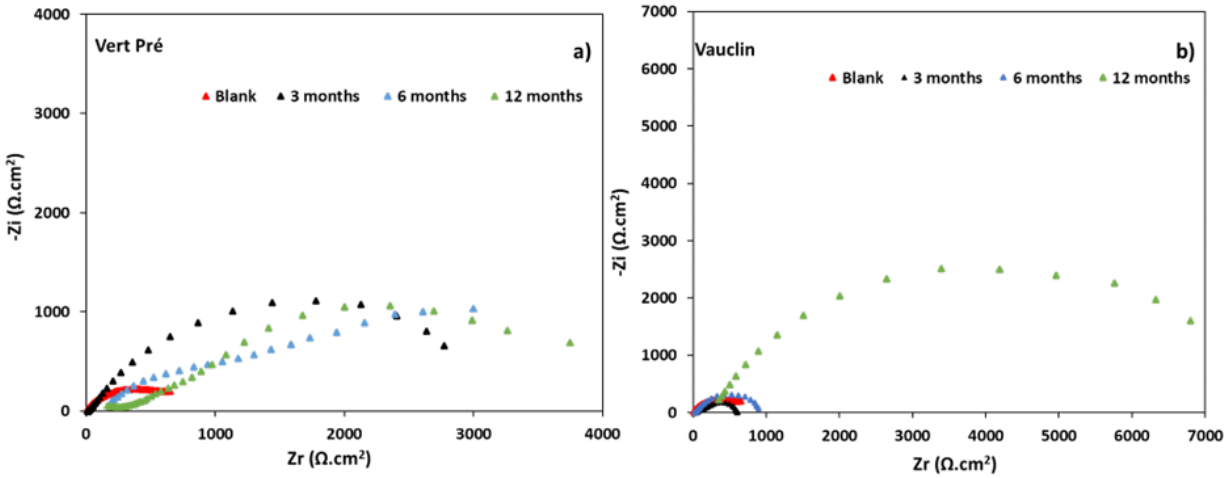

Figure 6. Nyquist plots in NaCl obtained for samples of Cu exposed in *Vert pré* (a) and *Vauclin* (b)

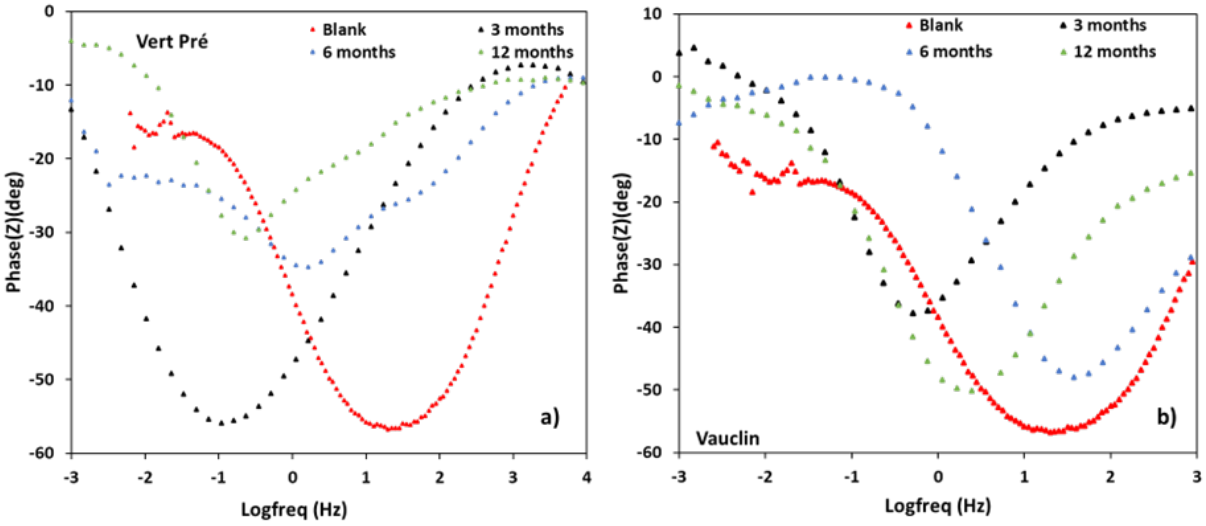

Figure 7. Bode plots in NaCl obtained for samples of Cu exposed in *Vert pré* (a) and *Vauclin* (b)

The electrochemical parameters obtained from the impedance spectra for samples exposed in *Vert pré* and Vauclin are listed in **Table 4**. It is notable that the values of R_{totale} increase significantly

with the duration of exposure, which is in accordance with the observed decrease in corrosion rate measured by gravimetry (**Table 2**). These corrosion surfaces then behave similarly to those exposed in a marine atmosphere. It can be concluded that low H_2S concentrations in a chloride-rich marine environment do not significantly alter the corrosion surface behavior.

In *Vauclin*, the obtained Nyquist diagrams also reveal the presence of a single large capacitive half-loop (**Figure 6b**), defined by a time constant in the Bode plot (**Figure 7b**). This means that only one phenomenon has occurred and is characteristic of the development of a corrosion product layer. We observed a significant increase in the diameter of the capacitive half-loops with the duration of exposure. This increase indicates an enhancement of the protective properties of the layer, as observed in the case of a marine atmosphere without H_2S (*Diamant*). These observations are consistent with morphological findings and corrosion products obtained in (Said Ahmed *et al.*, 2023). In this case, the Nyquist diagrams obtained were adjusted using an equivalent electrical circuit composed of an R/CPE element, as shown in **Figure 5b**. The Nyquist diagrams obtained for the samples exposed in *Vert pré*, presenting two capacitive loops, were adjusted using an equivalent electrical circuit composed of two R/CPE elements as shown in the **Figure 5a**.

Table 4. Electrochemical parameters obtained for samples exposed in Vauclin and Vert pré at different exposure durations

	Blank	***Vert pré***			***Vauclin***		
Months		3	6	12	3	6	12
R_e ($\Omega.cm^2$)	3	31	60	231	33	35	268
R_1($\Omega.cm^2$)	–	2542	1243	746	544	970	6525
n_1	–	0.6831	0.6704	0.6384	0.7501	0.7237	0.7034
$Q_1 10^{-4}$ ($\Omega^{-1}cm^{-2}s^{n1}$)	–	3.6	7	6	7.3	6.4	0.93
R_2($\Omega.cm^2$)	619	–	1757	3157	–	–	–
n_2	0.6978	–	0.7231	0.7354	–	–	–
$Q_2 10^{-4}$ ($\Omega^{-1}cm^{-2}s^{n2}$)	12	–	2.3	0.5	–	–	–
R_{total}($\Omega.cm^2$)	619	2542	3000	3903	544	970	6527

To support the EIS results, linear polarization was performed on the sample exposed in different sites. The polarization curves obtained are shown in **Figure 7**. The mechanism of anodic dissolution in the presence of chloride is well-known and is characterized by two successive steps described by **Eqn. 2 and 3.** The first step involves the formation of CuCl (adsorbed species) between the corrosion potential and 0.1 V/SCE, accompanied by the dissolution of copper in the form of $CuCl_2^-$ ions, followed by the dissolution of Cu (II) species for more anodic potentials. This reaction is under mixed activation-diffusion control.

$$Cu^+ + Cl^- \rightarrow CuCl \qquad \textbf{Eqn. 2}$$

$$Cu^+ + Cl^- \rightarrow CuCl_2^- \qquad \textbf{Eqn. 3}$$

The corrosion kinetics depend on both anodic and cathodic redox half-reactions. In aerated solution, the oxygen reduction reaction is favored. Corrosion current densities increase, making the

material more susceptible to corrosion. The reduction of oxygen thus plays a crucial role in the corrosion mechanism and kinetics. This cathodic reaction is considered the driving force of corrosion. In the cathodic branch, a substantially linear variation is observed from -0.23 V/SCE to -0.4 V/SCE, indicating the existence of a region controlled by kinetics. In the literature between -0.65 and -1.2 V/SCE, a diffusion plateau is observed, attributed to the transport of dissolved oxygen towards the electrode.

The polarization curves of copper samples exposed in a marine atmosphere with and without H_2S in *Diamant* and *Fregate est* are presented in the same **Figures 8 a-b**. In both cases, a decrease in cathodic and anodic current densities over time is observed. However, this decrease is more pronounced for samples exposed in an atmosphere without H_2S. Indeed, the formation of the corrosion layer decreases both the anodic partial current corresponding to metal dissolution and the cathodic partial current corresponding to the reduction of O_2 and/or dissolved HS^- in the electrolytic layer. Furthermore, in the absence of H_2S (*Diamant*), a shift of the corrosion potential towards negative values is observed. Whereas in an atmosphere rich in H_2S (*Fregate est*), it shifts towards positive values. This can be explained by the significant thickness of corrosion products obtained in this site.

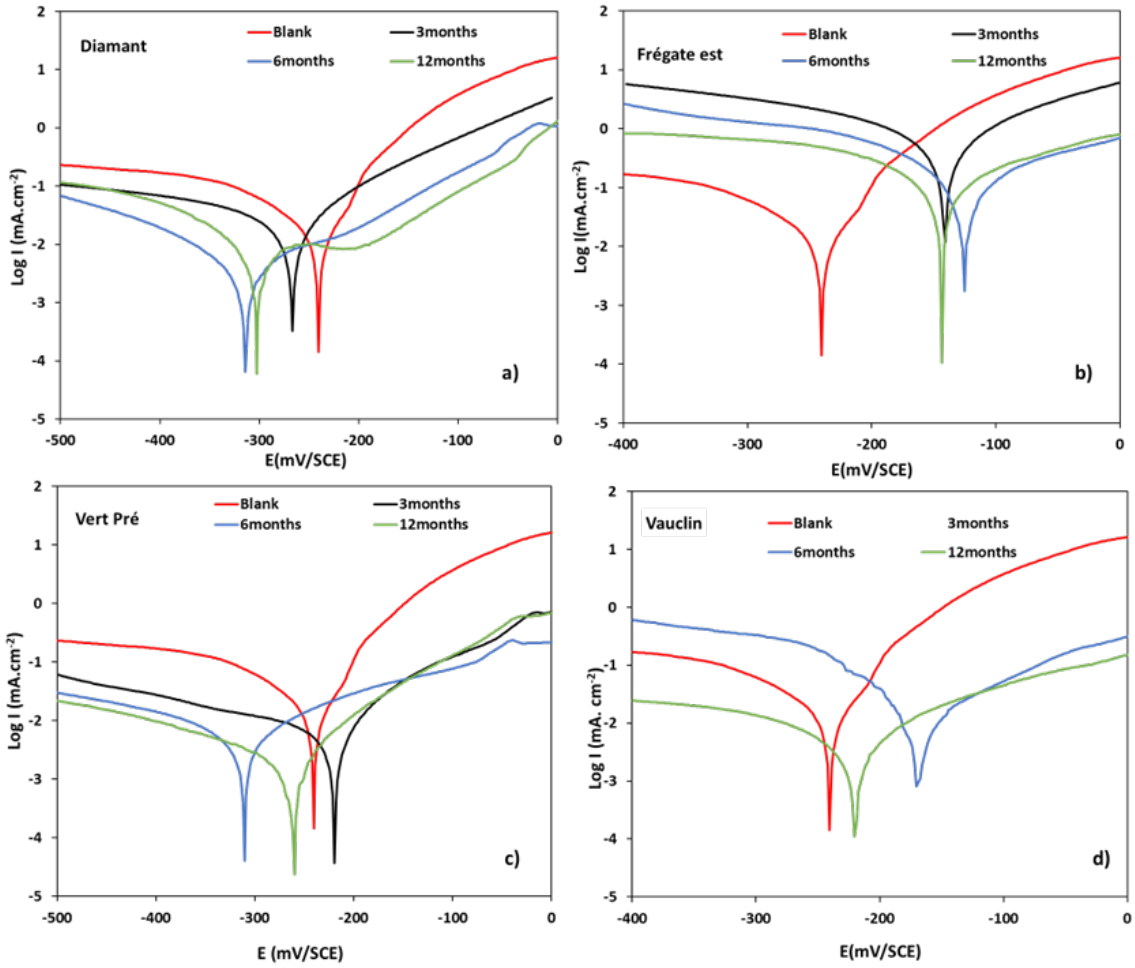

Figure 8. Polarization curves in NaCl obtained for samples of Cu exposed in a) *Diamant* b) *Fregate est* c) *Vert pré* d) *Vauclin* for 3 to 12 months

The polarization curves of samples exposed in *Vauclin* and *Vert pré* exhibit similar behaviors to those obtained for Diamant (**Figure 8 c-d**). However, the current densities are more impacted for the Vauclin site, which is consistent with gravimetric results indicating a higher corrosion rate.

It is also noteworthy that the anodic domain for all sites, except for *Fregate est*, is similar to that of the non-exposed copper and can be divided into two regions: the first corresponds to corrosion products (adsorbed species such as $Cu_2Cl(OH)_3$, etc.), accompanied by their dissolution. This dissolution is less pronounced for 3 months, probably due to the compactness of the film at this exposure time, and becomes more pronounced for 6 months, making the metal more susceptible to corrosion. This anodic behavior is characteristic of copper and certain copper alloys (Benedeti *et al.*, 1995).

The Table 5 regroups the electrochemical parameters obtained from polarization curves. The presented values are derived from the linear representations of *I–E* in the potential range ± 30 mV from the corrosion potential. Calculations cannot be performed using Tafel curves as the anodic and cathodic branches of the polarization curves do not exhibit the necessary linear portions required for Tafel line fitting. It is observed that polarization resistances increase with exposure time for all the studied sites, except for the Frégate est site (this increase is minor.). It is noteworthy that the polarization resistances of copper surfaces obtained in an atmosphere without H_2S (Diamant) are significantly higher and increase over time. These results corroborate those obtained through impedance measurements and the corrosion rates observed for this site. The results of potentiodynamic polarization are fully consistent with the electrochemical impedance spectroscopy (EIS) analysis, confirming the reliability of the electrochemical measurements. Therefore, the presence of H_2S diminishes the anti-corrosive performance of copper and leads to more significant corrosion.

Table 5. Electrochemical parameters obtained from Polarization

Months		E_{corr}	R_p	I_{corr}
		mV/SCE	Ω.cm²	mA.cm⁻²
Blank		-241	855	29
Diamant	3	-269	1140	22
	6	-313	5438	4.7
	12	-286	9513	2.7
Frégate est	3	-139	62	417
	6	-124	177	147
	12	-143	194	134
Vert Pré	3	-222	3145	8.2
	6	-311	4463	5.8
	12	-263	9645	2.7
Vauclin	3	-199	260	100
	6	-166	1252	20
	12	-221	4928	5.2

4. Conclusion

In this study, the atmospheric corrosion of copper, at four sites with varying degrees of impact from *Sargassum algae* strandings, was evaluated. The *Frégate est* site exhibited the highest concentrations of H_2S, whereas the *Diamant* site recorded the highest concentrations of chlorides.

These identified atmospheric models were thoroughly examined, and the obtained results were compared to those from two other sites (*Vauclin* and *Vert pré*).

Indeed, two electrochemical behaviors were established, with or without H_2S. In the first case (*Frégate est*, with H_2S), the values of total resistance and polarization resistance of the corrosion surface were very low. This indicates that the corrosion products formed provide very little protection to the metal surface. This behavior was explained by the non-adherence of CuS to the corrosion surface. In the second case, the presence of Cu_2O decreased the conductance of the corrosion surface. These results were confirmed by the very high resistances obtained. This behavior intensifies with the exposure time. A similar electrochemical behavior to the latter was obtained for the *Vert pré* and *Vauclin* sites. The potentiodynamic polarization results closely align with the EIS analysis, confirming the reliability of the electrochemical measurements. As a result, the presence of H_2S diminishes the anti-corrosive effectiveness of copper, leading to increased corrosion.

Disclosure statement: *Conflict of Interest:* The authors declare that there are no conflicts of interest.
Compliance with Ethical Standards: This article does not contain any studies involving human or animal subjects

5. References

Bai, Z., Li, X., Feng, Y., Qiong, Y., Junshenh, W., Dong, S., Kui, X. (2022) Atmospheric Corrosion of Copper by an Acid-Producing Aspergillus versicolor in the Presence of Chloride, *J. Mater. Eng. Perform.,* 32, 6677-6685.

Becker, J., Pellé, J., Rioual, S., Lescop, B., Le Bozec, N., Thierry, D. (2022) Atmospheric corrosion of silver, copper and nickel exposed to hydrogen sulphide: a multi-analytical investigation approach, *Corros. Sci.*, 209, 110726.

Benedeti, A. V., Sumodjo, P. T. A., Nobe, K., Cabot, P. L., Proud, W. G. (1995) Electrochemical studies of copper, copper-aluminium and copper-aluminium-silver alloys: Impedance results in 0.5M NaCl, *Electrochem. Acta*., 40, 2657-2668.

Cai, Y., Xu, Y., Zhao, Y., Ma, X. (2020) Atmospheric corrosion prediction: A review, *Corros. Rev*. 38, 299-321.

Cai, Y.K., Zhao, Y., Ma, X.B., Zhou, K., Chen, Y. (2018) Influence of environmental factors on atmospheric corrosion in dynamic environment, *Corros. Sci*., 137, 163-175.

Cramer, S. D., McDonald, L. G., Atmospheric factors affecting the corrosion of zinc, galvanized steel, and copper (1990) *ASTM-STP 1000*, *ASTM*, Philadelphia, PA., 241-259.

Dafali A., Hammouti B., Touzani R., Kertit S., Ramdani A., Elkacemi K. (2002), Corrosion Inhibition of copper in 3% NaCl solution by new bipyrazolic derivatives, *Anti-corros. Meth. & Mat.,* 49N°2, 96-104.

Deslouis, C., Tribollet, B., Mengoli, G., Musiani, M, M. (1988) Electrochemical behaviour of copper in neutral aerated chloride solution. II. Impedance investigation, *J. Appl. Electrochem*., 18, 384-393.

Dueke Eze C. U., Madueke N. A., Iroha N. B., Maduelosi N. J., Nnanna L. A., *et al.* (2022) Adsorption and inhibition study of N-(5-methoxy-2-hydroxybenzylidene) isonicotinohydrazide Schiff base on copper corrosion in 3.5% NaCl, *Egypt. J. Pet.,* 31, 31 -37

Feliu, S., Morcillo, M., Feliu, S, Jr. (1993) The prediction of atmospheric corrosion from meteorological and pollution parameters. II: Long-term forecasts, *Corros. Sci*, 34, 415-422.

Gourbeyre, Y., Tribollet, B., Dagbert, C., Hyspecka, L. (2006) A physical model for anticorrosion behavior of duplex coatings, *J. Electrochem. Soc*.,153.

Guttman, H. (1982) Atmospheric and weather factors in corrosion testing. Atmospheric Corrosion, *John Wiley & Sons, Inc*.

Kucera, V., Mattsson, E., (1987) Atmospheric corrosion. F. *Mansfeld (Ed.), Corrosion Mechanisms, Marcel Dekker, Inc,* New York., 211-284.

Leygraf, C., Wallinder, I.O., Tidblad, J., Graedel, T. (2016) Atmospheric corrosion. *John Wiley & Sons*, Hoboken, NJ, USA.

Love, J. C., Estroff L. A., Kriebel J. K., Nuzzo R. G., Whitesides G. M. (2005) Self-assembled monolayers of thiolates on metals as a form of nanotechnology, *Chem Rev.* 105(4):1103-69.

Lu, X., Liu, Y., Zhao, H., Pan, C., Wang, Z. (2021) Corrosion behavior of copper in extremely harsh marine atmosphere in Nansha Islands, China, *Trans. Nonferrous Met. Soc. China*, 31, 703-714.

Mihit M., Salghi R., El Issami S., Bazzi L., Hammouti B., Ait Addi, El. Kertit S. (2006), A study of tetrazoles derivatives as corrosion inhibitors of copper in nitric acid, *Pigm. Resin Technol*. 35 N° 3, 151-157.

Odnevall, D., Leygraf, C. November (1996) The atmospheric corrosion of copper-a multianalytical approach. Proceedings of 13th International, *Corrosion Congress, Melbourne Australia*.

Pareek S., Jain D., Hussain S., Biswas A., Shrivastava R., Parida S. K., Kisan H. K., Lgaz H., Chung I-M., Behera D. (2019), A new insight into corrosion inhibition mechanism of copper in aerated 3.5 wt.% NaCl solution by eco-friendly Imidazopyrimidine Dye: experimental and theoretical approach, Chemical Engineering Journal, Volume 358, 2019, 725-742, ISSN 1385-8947, https://doi.org/10.1016/j.cej.2018.08.079

Pawara, P., Gaikwad, B., Patil, P. P. (2007) Corrosion protection aspect of electrochemicaly synthesized poly(o-anisidine-co-o-toluidine) coatings on copper, *Electrochem. Acta*., 52, 5958-5967.

Said Ahmed, M., Lebrini, M., Lescop, B., Pellé, J., Rioual, S., Amintas, O., Roos, C. (2023) Corrosion of Copper in a Tropical Marine Atmosphere Rich in H_2S Resulting from the Decomposition of Sargassum Algae, *Metals*, 13, 982.

Sedik, A., Athmani, S., Saoudi, A., Ferkous, H., Ribouh, N., *et al.* (2022) Experimental and theoretical insights into copper corrosion inhibition by protonated amino-acids, *RSC Adv.*, 12, 23718-23735.

Vera, R., Araya, R., Bagnara, M., Diaz-Gomez, A., Ossandon, S. (2017) Atmospheric corrosion of copper exposed to different environments in the region of Valparaiso, Chile, *Mater. Corros*. 68, 316-328.

Wan, S., Hou, J., Zhang, Z. F., Zhang, X., Dong, Z. H. (2019) Monitoring of atmospheric corrosion and dewing process by interlacing copper electrode sensor, *Corros. Sci.,* 150, 246-257.

Xuankai, W., Yi, X., Chao, F., Zhimin, D., Dengke, L., Xiaobao, Z., Tangqing, W. (2022) Atmospheric corrosion of tin coatings on H62 brass and T2 copper in an urban environment, *Eng. Fail. Anal.*, 141, 106735.

Zschieschang U., Ante F., Schlörholz M., Schmidt M., Kern K., Klauk H. (2010) Mixed Self-Assembled Monolayer Gate Dielectrics for Continuous Threshold Voltage Control in Organic Transistors and Circuits, *Advanced Materials*, 40, 4489.